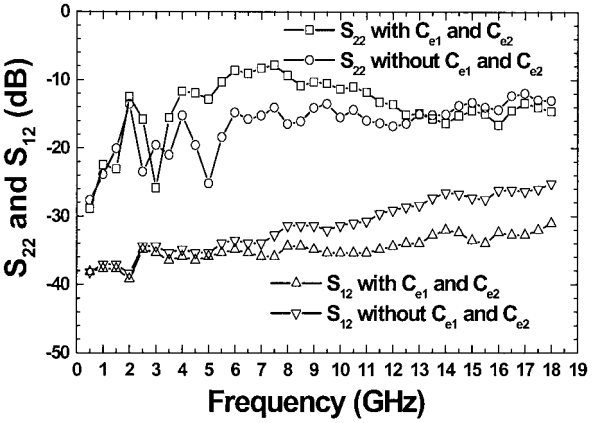

Figure 4 Measurement results of reverse-transmission gain and output-return loss for GaInP/GaAs HBT wideband amplifiers with and without emitter peaking

$$Z_T = \frac{S_{21}}{1 - S_{11}} \cdot 50.$$

The circuit using emitter-gain-peaking capacitors has 65-dBΩ gain and 8-GHz 3-dB bandwidth for Z_T, but the circuit without emitter-peaking capacitors has the same gain with 4-GHz 3-dB bandwidth for Z_T. The Z_{21} data in Figure 5 also shows that the emitter-peaking capacitors have an influence upon the Z_{21} response. Figure 6 illustrates the noise and power performances of both circuits. Both designs have similar noise figures, which are less than 2.8 dB for frequencies below 6 GHz. OP_{1dB} and OIP_3 of both circuits as functions of frequency are also illustrated in Figure 6. OP_{1dB} and OIP_3 are 7 and 20 dBm at 2 GHz, respectively. Both OP_{1dB} and OIP_3 decrease when the frequency increases. There is no apparent power-performance difference between the two designs.

4. CONCLUSION

In this paper, 28-dB gain, DC to 6-GHz GaInP/GaAs shunt-series shunt-shunt feedback wideband amplifiers have been demonstrated. The experimental results show that power gain is 28 dB and input/output return loss is below 12 dB from DC to 6 GHz for the wideband amplifier without emitter-capacitive peaking. An emitter-capacitive peaking technique can extend the 3-dB power-gain bandwidth at the cost of lower input/output return loss. The

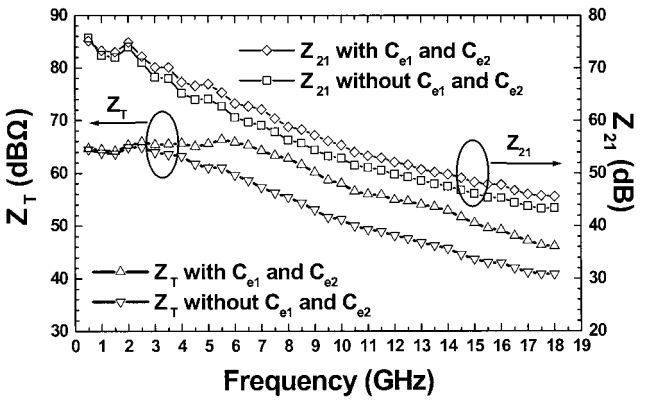

Figure 5 Measured Z_T and Z_{21} of GaInP/GaAs HBT wideband amplifiers with and without emitter peaking

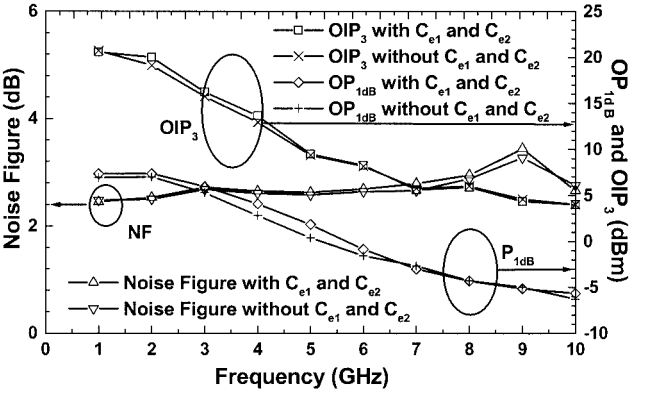

Figure 6 Measured noise figures and power performances of GaInP/GaAs HBT wideband amplifiers with and without emitter peaking

circuit using peaking capacitors has 8-GHz 3-dB power-gain bandwidth, while S_{11} reaches −8 dB and S_{22} reaches −9 dB at 8 GHz. Both circuits have similar noise and power performances. The noise figures of both circuits are less than 2.8 dB for frequencies below 6 GHz.

ACKNOWLEDGMENTS

This work was supported by the National Science Council of Republic of China under grant no. NSC 92-2219-E-009-023 and by the Ministry of Education under grant no. 89-E-FA06-2-4.

REFERENCES

1. R.G. Meyer and R.A. Blauschild, A 4-Term wide-band monolithic amplifier, IEEE J Solid State Circ SC-16 (1981), 634–638.
2. C.D. Hull and R.G. Meyer, Principles of monolithic wideband feedback amplifier design, J High-Speed Electron 3 (1992), 53–93.
3. K.W. Kobayashi and A.K. Oki, A DC-10 GHz high gain-low noise GaAs HBT direct-coupled amplifier, IEEE Microwave Guided Wave Lett 5 (1995).
4. K.W. Kobayashi and A.K. Oki, A low-noise baseband 5-GHz direct-coupled HBT amplifier with common-base active input match, IEEE Microwave Guided Wave Lett 4 (1994).
5. M.C. Chiang, S.S. Lu, C.C. Meng, S.A. Yu, S.C. Yang, and Y.J. Chan, Analysis, design, and optimization of InGaP-GaAs HBT matched-impedance wideband amplifiers with multiple feedback loops, IEEE J Solid States Circ 37 (2002), 694–701.

TENSOR PRODUCT DERIVATIVE MATCHING FOR WAVE PROPAGATION IN INHOMOGENEOUS MEDIA

Shan Zhao[1] and G. W. Wei[1,2]
[1] Department of Mathematics
Michigan State University
East Lansing, MI 48824
[2] Department of Electrical and Computer Engineering
Michigan State University
East Lansing, MI 48824

Received 10 March 2004

ABSTRACT: *We propose a tensor product derivative matching (TPDM) method to restore the accuracy of high-order finite difference time-domain (FDTD) schemes of computational electromagnetics (CEM)*

with material interfaces in two spatial dimensions (2D). By making use of fictitious points, the TPDM method locally enforces the physical-jump conditions at material interfaces in a preprocessing stage to arbitrarily high orders of accuracy in principle, based on a structured grid. The proposed method encompasses a variety of schemes of different orders in a single code. In fact, numerical orders from 2 to near 16 are confirmed in the present study. To the best of our knowledge, such high orders have not been reported in the literature for CEM problems involving material interfaces. The limitation and applicability of the present scheme are also analyzed in detail. © 2004 Wiley Periodicals, Inc. Microwave Opt Technol Lett 43: 69–77, 2004; Published online in Wiley InterScience (www.interscience.wiley.com). DOI 10.1002/mop.20378

Key words: *Maxwell's equations; finite-difference time-domain methods; material interfaces; high-order methods*

1. INTRODUCTION

The finite-difference time-domain (FDTD) method was proposed by Yee [1] near forty years ago and was generalized by Taflove [2] and many others [3–19]. Although the original FDTD method is very simple, free of dissipative error, and has very low cost per grid node, it suffers from high dispersive error [3], and severe accuracy reduction at geometries and material interfaces [4]. Much improvement has been made in the past two decades to improve the staircased approximation for boundaries and geometries [5–7] to reduce the dispersive error [3, 8–17] and to restore the accuracy at material interfaces [4, 18, 19]. As a result, FDTD methods are now the main workhorse of computational electromagnetics (CEM) in the time domain for a variety of scientific and engineering applications in micro/nano devices, near field optics, antennas, radar cross section, wave propagation and scattering. However, for electromagnetic wave propagation involving high frequency waves and/or large domain, the present FDTD techniques are insufficient. There is still a pressing need for a generalized FDTD method which is of high order, and thus well suitable for large scale computations involving complex geometries, boundaries, and material interfaces. Here, by high order, we refer to schemes that are of order four or higher.

Important contributions to the field were made by Yefet and Turkel [20], Yefet and Petropoulos [21], Xie, Chan and Zhang [22, 23], and Hesthaven [4], who generalize the embedding schemes [4, 18, 19] to fully fourth-order FDTD methods on a simple structured grid with material interfaces. The significant achievements of these high-order embedding schemes [20–23] is that they enforce physical jump conditions at material interfaces up to high-order at a preprocessing stage, so that fourth-order convergence is uniformly assured over the entire domain. Subtle interface techniques with one-sided difference approximations and extrapolations are required in these methods. We refer to a recent review [4] for the accomplishment, difficulty, and challenge in high-order time-domain methods.

The feasibility of extending the previous embedding FDTD schemes beyond the 4^{th} order for treating material interfaces was not very clear [4] until the most recent work [24], which achieved more than 10^{th}-order accuracy. Motivated by the use of fictitious points (FPs) in a block pseudospectral (BPS) method [25, 26], a hierarchical derivative matching (HDM) method [24] was proposed to systematically enforce the physical-jump conditions at material interfaces to arbitrary orders of accuracy in principle. Nevertheless, we note that the recursive nature of the HDM scheme restraints its ability for attaining 12^{th} orders for a few test examples. It is therefore of great interest to develop a systematic approach to correctly enforce the physical-jump conditions at material interfaces to even higher orders. To this end, we present herein a tensor-product derivative matching scheme, which can greatly exceed the numerical order attained by the previous FDTD methods.

This paper is organized as follows. Section 2 is devoted to the theory and algorithm. A brief description of Maxwell's equations and boundary conditions is presented to introduce the problem. A short review is given to an implicit derivative matching (IDM) method, which underpins the theoretical foundation of both the previous HDM and the present TPDM method. The latter is described in detail. Numerical experiments are carried out to validate the proposed method in section 3. The limitation of the approach is also analyzed in detail, followed by the conclusion.

2. THEORY AND ALGORITHM

For the sake of integrity and establishing notation, we review the method of implicit derivative matching in 1D cases [24] before the TPDM method is introduced.

2.1 Governing Equations and Boundary Conditions

To illustrate our method, it is sufficient to consider the vector form of the time-dependent Maxwell's equations

$$\frac{\partial \mathbf{q}}{\partial t} = A\mathbf{q}, \tag{1}$$

where

$$\mathbf{q} = \begin{bmatrix} E_z \\ H_y \end{bmatrix}, \quad A = \begin{bmatrix} 0 & \frac{1}{\varepsilon}\frac{\partial}{\partial x} \\ \frac{1}{\mu}\frac{\partial}{\partial x} & 0 \end{bmatrix} \tag{2}$$

for the 1D modeling and

$$\mathbf{q} = \begin{bmatrix} H_x \\ H_y \\ E_z \end{bmatrix}, \quad A = \begin{bmatrix} 0 & 0 & -\frac{1}{\mu}\frac{\partial}{\partial y} \\ 0 & 0 & \frac{1}{\mu}\frac{\partial}{\partial x} \\ -\frac{1}{\varepsilon}\frac{\partial}{\partial y} & \frac{1}{\varepsilon}\frac{\partial}{\partial x} & 0 \end{bmatrix} \tag{3}$$

for the 2D study. Here, E_z and H_α ($\alpha = x, y$) are components of the electric- and magnetic-field intensities, respectively, ε and μ are the electric permittivity and magnetic permeability, respectively. A nondimensional form of the equations is considered, that is, $\varepsilon = \mu = 1$ in free space.

When there is material interfaces, the solution to the transverse electromagnetic (TEM) mode [Eq. (2)] and transverse magnetic (TM) mode [Eq. (3)] requires special treatment in order to attain high orders. At an interface between two media, say, medium 1 and medium 2, the boundary conditions can be expressed mathematically as

$$\hat{\mathbf{n}} \times (\mathbf{E}_1 - \mathbf{E}_2) = \mathbf{0}, \quad \hat{\mathbf{n}} \times (\mathbf{H}_1 - \mathbf{H}_2) = \mathbf{0}, \tag{4}$$

for electric fields and magnetic fields, respectively. Here $\hat{\mathbf{n}}$ is the unit vector normal to the interface, pointing from medium 2 into medium 1. A special case with one of the media, say medium 2, being a perfect electric conductor (PEC), is of practically importance. The PEC boundary conditions reduce to a simple form, given by

$$\hat{\mathbf{n}} \times \mathbf{E} = \mathbf{0}, \tag{5}$$

since a perfect conductor cannot sustain a field inside.

2.2 Method of Implicit Derivative Matching

We start with simple 1D cases to introduce our scheme. We assume that the 1D domain under study consists of two dielectric media, with the interface at $x = \xi$. As a result, the coefficient matrix A of Eq. (1) takes different values in media 1 and 2, that is, $A = A_1$ if $x < \xi$ and $A = A_2$ if $x > \xi$. We impose physical-jump conditions of order p at the interface

$$A_1^p \mathbf{q}(\xi^-, t) = A_2^p \mathbf{q}(\xi^+, t), \quad p = 0, 1, 2, \ldots, \tag{6}$$

where

$$A_1^p \mathbf{q}(\xi^-, t) = [A_1^p \mathbf{q}(x, t)]_{x \to \xi^-}, \quad A_2^p \mathbf{q}(\xi^+, t) = [A_2^p \mathbf{q}(x, t)]_{x \to \xi^+}.$$

These jump conditions relate the electromagnetic fields across the interface and their derivatives as taken from two sides of the interface. These conditions are the starting point for constructing the method of implicit derivative matching (IDM) [24]. We use Figure 1 to illustrate our idea. Let us denote the function values under consideration (either E_z or H_y) at original and fictitious points as g_i and f_i (for $i = 1, 2, \ldots, 2m$), respectively. For simplicity, a uniform, staggered grid is assumed in the present study. It is important to note that the interface $x = \xi$ needs not to be laid on the grid in the IDM method. For a given number of FPs, m, up to $(2m - 1)^{\text{th}}$-order physical-jump conditions are employed to determine the representation weights of $2m$ FPs. As in our previous work [24], standard central finite-difference (FD) approximations are utilized to discretize these $2m$ jump conditions. The resultant discretized equations then are evaluated at each grid point to form $2m \times 2m$ algebraic equations, which could be solved to determine $2m \times 2m$ unknowns.

To illustrate the idea, we consider the second-order jump condition for E_z,

$$\frac{1}{\varepsilon_1} E_z^{(2)}(\xi^-, t) = \frac{1}{\varepsilon_2} E_z^{(2)}(\xi^+, t), \tag{7}$$

where the superscript denotes the 2nd-order derivative. Eq. (7) can be discretize by using the FD approximation

$$\frac{1}{\varepsilon_1}\left[\sum_{i=1}^{m} w_{2,i} g_i + \sum_{i=m+1}^{2m} w_{2,i} f_i\right] = \frac{1}{\varepsilon_2}\left[\sum_{i=1}^{m} w_{2,i} f_i + \sum_{i=m+1}^{2m} w_{2,i} g_i\right], \tag{8}$$

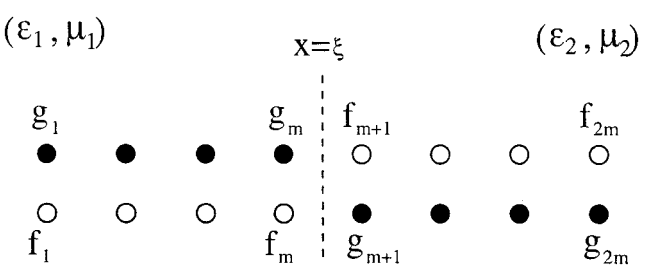

Figure 1 Illustration of FPs and notation used in the IDM method

where $w_{2,i}$, $i = 1, 2, \ldots, 2m$, are the standard FD weights for the 2nd-order derivative approximation. It is obvious from Eq. (8) that the splitting in the summation reflects the division over the interface (see Fig. 1). We note that, since a uniform grid and the central scheme are used, the sets of FD weights of the left- and right-hand sides of Eq. (8) are the same.

The rest of the job is to derive a set of desired algebraic equations for being used in an implicit scheme. To this end, we rewrite Eq. (8) as

$$\frac{1}{\varepsilon_1} \sum_{i=m+1}^{2m} w_{2,i} f_i - \frac{1}{\varepsilon_2} \sum_{i=1}^{m} w_{2,i} f_i = \frac{1}{\varepsilon_2} \sum_{i=m+1}^{2m} w_{2,i} g_i - \frac{1}{\varepsilon_1} \sum_{i=1}^{m} w_{2,i} g_i. \tag{9}$$

Note that the right-hand side of Eq. (9) contains known values.

We look for a preprocessing scheme so that it is *not* necessary to resolve f_i at each time step. To this end, let us write

$$f_i = \sum_{j=1}^{2m} r_{i,j} g_j, \quad \text{for } i = 1, 2, \ldots, 2m, \tag{10}$$

where $r_{i,j}$ are representation coefficients. It is convenient to adopt a matrix representation for Eq. (10), given by

$$F = RG, \tag{11}$$

where $F = (f_1, f_2, \ldots, f_{2m})^T$, $G = (g_1, g_2, \ldots, g_{2m})^T$, and $R = (r_{i,j})_{i,j=1}^{2m}$. Our task is to determine the unknown coefficient matrix R. It is convenient to consider the rows of R as new variables, $R_j = (r_{j,1}, r_{j,2}, \ldots, r_{j,2m})$ for $j = 1, 2, \ldots, 2m$. To determine the coefficients/elements of R is equivalent to solve a vector $\hat{R}$, given by

$$\begin{aligned}\hat{R} &= (R_1, R_2, \ldots\ldots, R_{2m})^T \\ &= (r_{1,1}, r_{1,2}, \ldots, r_{1,2m}, r_{2,1}, r_{2,2}, \ldots, r_{2,2m}, \ldots\ldots, r_{2m,1}, \\ &\qquad r_{2m,2}, \ldots, r_{2m,2m})^T\end{aligned} \tag{12}$$

from an algebraic system. It is noted that the dimension of the matrix system for determining $\hat{R}$ is $(2m)^2$, which is high when m is large. To resolve f_j and g_j, we define $2m$ vectors I_j as the rows of a $2m \times 2m$ identity matrix I, that is, $I_1 = (1, 0, 0, \ldots, 0)$, $I_2 = (0, 1, 0, \ldots, 0)$, $\cdots I_{2m} = (0, 0, 0, \ldots, 0, 1)$. This leads to the following symbolical representations:

$$f_j = R_j G \quad \text{and} \quad g_j = I_j G. \tag{13}$$

Substituting two relations in Eq. (13) into Eq. (9), we obtain

$$\begin{aligned}\frac{1}{\varepsilon_1} \sum_{i=m+1}^{2m} w_{2,i} R_i G - \frac{1}{\varepsilon_2} \sum_{i=1}^{m} w_{2,i} R_i G \\ = \frac{1}{\varepsilon_2} \sum_{i=m+1}^{2m} w_{2,i} I_i G - \frac{1}{\varepsilon_1} \sum_{i=1}^{m} w_{2,i} I_i G.\end{aligned} \tag{14}$$

Finally, by eliminating the common abstract variable G, we end up with $2m$ algebraic equations from the jump condition of Eq. (7):

$$\frac{1}{\varepsilon_1}\sum_{i=m+1}^{2m} w_{2,i}R_i^T - \frac{1}{\varepsilon_2}\sum_{i=1}^{m} w_{2,i}R_i^T = \frac{1}{\varepsilon_2}\sum_{i=m+1}^{2m} w_{2,i}I_i^T - \frac{1}{\varepsilon_1}\sum_{i=1}^{m} w_{2,i}I_i^T. \tag{15}$$

These equations have the desirable feature of being independent of the field values. Therefore, they can be used in a preprocessing stage. Algebraic equations for other jump conditions can be similarly derived.

It is interesting to note that the function values on FPs, that is, $\{f_i\}_{i=1}^{2m}$, are never evaluated in the present study. By means of representation coefficients $r_{i,j}$, we locally modify the differential stencil near the material interface at the beginning of the computation, as in the embedding FDTD schemes [4, 18–23]. Therefore, this method is referred as an implicit derivative matching (IDM) [24].

2.3 Derivative Matching in Higher Dimensions

We focus mainly on the 2D studies in the present paper. It is noted that the idea underlying the present 2D studies can be similarly extended to a general 3D scenario. In a 2D domain, it is supposed that the media are nonmagnetic with $\mu = 1$ and are homogeneous in the y direction. Similar to the 1D cases, the electric permittivity ε is a piecewise constant with two values ε_1 and ε_2 in the x direction. Again, we assume that the interface is at $x = \xi$. The case in which there are multiple interfaces can be similarly treated. The notations for A_1 and A_2 can be similarly defined. Following the convention of CEM, a 2D staggered grid is used for the fields E_z, H_x, and H_y [2, 15, 16].

We first establish physical-jump conditions at $x = \xi$. It is worthwhile to note that we have three conditions for three field components in each order of jump conditions. Among them, only two conditions are employed in the DM modeling, because such a modeling is carried out for E_z and H_y only. For the field component H_x, since a derivative of H_x with respect to x is not required to be evaluated in the resolution of the TM equations (1) and (3), it is not necessary to conduct a DM modeling for H_x. In general, the n^{th}-order jump condition is given as

$$A_1^n\mathbf{q}(\xi^-, t) = A_2^n\mathbf{q}(\xi^+, t), \tag{16}$$

where the 0^{th}-order jump condition states that the fields are continuous across the following interface:

$$\mathbf{q}(\xi^-, t) = \mathbf{q}(\xi^+, t). \tag{17}$$

For each n, there are a set of three equations. The first two sets of matching conditions can be easily implemented numerically. However, starting from $n = 2$, one encounters terms with cross derivatives, such as $(\partial^2/\partial x\partial y)H_y$, that are required to be discretized. To approximate a cross derivative with the respective lengths of differential kernels given by $2M_x$ and $2M_y$, respectively, a total number of $4M_xM_y$ grid points is involved. Obviously, the computational cost is then extremely high, especially when M_x and M_y are quite large.

Two methods, a quasi-4^{th}-order derivative matching (Q4DM) scheme and a 2D hierarchical derivative matching (HDM) method, were proposed to overcome the aforementioned difficulty [24]. The Q4DM is a direct extension of the 1D IDM scheme, that is, symmetric FD weight functions are used with fictitious grid points to attain high-order accuracy. To avoid the cross derivatives, terms in the jump conditions that involve only derivatives normal to the interface are discretized with both appropriate fictitious grid points and original grid points. While other terms that involve derivatives tangential to the interface are discretized on the original grid points. Numerical tests indicate that the Q4DM is essentially of 4^{th} order in accuracy. The possibility of extending the Q4DM scheme to higher orders was examined. Apart from the associated complexity, such a generalization considering high-order jump conditions might not be able to achieve a high order of convergence eventually, simply because the increasing number of cross derivatives being discretized on the original grid are actually discontinuous across the interface.

The 2D HDM is an iterative scheme for gaining high-order accuracy. At each stage of the iteration, four jump conditions are employed, that is, the 0^{th}- and 1^{st}-order jump conditions of H_y and the 1^{st}- and 2^{nd}-order jump conditions of E_z. The x direction derivatives involved in these four conditions are discretized via one-sided FD approximations. Apart from that, two y direction derivatives also involve in these conditions, that is, $(\partial/\partial y)H_x(\xi)$ and $(\partial^2/\partial y^2)E_z(\xi)$. Note that these two terms are continuous at

TABLE 1 L_2 Errors of the FDTD Methods with the TPDM at Time $t = 1$ with $\Delta t = 2.5 \times 10^{-4}$ ($M_y = 8$)

		E_z		H_x		H_y	
M_x	(N_x, N_y)	Error	Rate	Error	Rate	Error	Rate
1	(26, 21)	1.57(−2)		5.96(−3)		1.64(−2)	
	(51, 41)	3.93(−3)	1.983	1.52(−3)	1.967	4.22(−3)	1.956
	(101, 81)	9.99(−4)	1.993	9.63(−5)	1.996	2.67(−4)	1.994
2	(26, 21)	3.53(−4)		1.38(−4)		3.97(−4)	
	(51, 41)	2.25(−5)	3.970	8.70(−6)	3.985	2.52(−5)	3.978
	(101, 81)	1.42(−6)	3.995	5.45(−7)	3.996	1.58(−6)	3.993
4	(26, 21)	4.10(−7)		1.61(−7)		4.80(−7)	
	(51, 41)	1.66(−9)	7.949	6.46(−10)	7.964	1.94(−9)	7.953
	(101, 81)	6.56(−12)	7.984	2.54(−12)	7.992	7.63(−12)	7.988
6	(26, 21)	6.84(−10)		2.71(−10)		8.20(−10)	
	(51, 41)	1.73(−13)	11.948	6.76(−14)	11.969	2.07(−13)	11.949
	(101, 81)	1.33(−14)	3.705	5.68(−15)	3.573	1.11(−14)	4.219
8	(26, 21)	1.32(−12)		5.28(−13)		1.62(−12)	
	(51, 41)	9.17(−15)	7.169	4.16(−15)	6.990	9.29(−15)	7.447
	(101, 81)	1.44(−14)	−0.650	5.19(−15)	−0.320	1.05(−14)	−0.182

the interface $x = \xi$. For simplicity, we assume that the interface $x = \xi$ is laid on some E_z nodes. By using such a body-conformed structured grid, the evaluation of two y derivatives can be quite straightforward and extremely accurate. Nevertheless, it is also noted that the HDM scheme is not suitable for general Cartesian grids. It is only applicable to body-conformed structured grids. In the previous numerical study, it was found that the 2D HDM scheme could attain as high as the 12th-order for wave propagation over interfaces. However, the accuracy was limited by the iterative nature of the scheme. Therefore, we propose an alternative approach in the next subsection.

2.4 Tensor-Product Derivative Matching Scheme

It is commented in the 1D BPS method [25] that it is straightforward to extend the explicit DM method into tensor-product domains in higher dimensions. However, an alternative DM modeling is conducted in the 2D BPS studies [26]. This may be due to great difficulties associated with the 2D DM modeling involving mixed derivatives, as discussed in detail in [24]. In this subsection, we further explore the extension of the 1D DM method to higher dimensions by using the principle of tensor products.

We start by a careful investigation to the general form of the analytical solution of 2D Maxwell's equations (1) and (3). For simplicity, we only consider E_z component in the present discussion. Suppose the electric-field density $\mathbf{E} = (E_x, E_y, E_z)$ is time harmonic, and can be represented as a plane-wave form, given by

$$E_z(x, y, t) = A \exp(i\omega_x x + i\omega_y y + i\omega t), \tag{18}$$

where ω_x and ω_y are the x- and y-components of physical wavenumber, and ω is the wave angular frequency. For TM modes, one general form of the analytical solutions of Eq. (1) can be given as

$$E_z(x, y, t) = A \sin(\omega_x x)\sin(\omega_y y)\cos(\omega t), \tag{19}$$

which is only one component of the plane wave Eq. (18), and with appropriate scaling, it is easy for E_z in Eq. (19) to satisfy the PEC conditions at boundaries.

On the other hand, it can be derived from Maxwell's equations (1) that E_z satisfies the 2D wave equation

$$\varepsilon \frac{\partial^2 E_z}{\partial t^2} = \frac{\partial^2 E_z}{\partial x^2} + \frac{\partial^2 E_z}{\partial y^2}. \tag{20}$$

By substituting Eq. (19) into Eq. (20), it can be derived that

$$\varepsilon\omega^2 = \omega_x^2 + \omega_y^2.$$

In general, ω is a scalar. For the present domain setting, we know that ε is invariant along the y direction, so that ω_y is a constant everywhere. Along the x direction, the electric permittivity ε is a piecewise constant with two values: ε_1 and ε_2. Therefore, there are two corresponding ω_x values and they satisfy

$$\varepsilon_1\omega^2 = \omega_{x,1}^2 + \omega_y^2,$$

$$\varepsilon_2\omega^2 = \omega_{x,2}^2 + \omega_y^2.$$

Correspondingly, the field E_z can be rewritten as

$$E_z(x, y, t) = \begin{cases} A_1\sin(\omega_{x,1}x)\sin(\omega_y y)\cos(\omega t) & \text{for } x < \xi, \\ A_2\sin(\omega_{x,2}x)\sin(\omega_y y)\cos(\omega t) & \text{for } x > \xi. \end{cases} \tag{21}$$

Based on the solution form of Eq. (21), we investigate the physical-jump conditions of E_z. As discussed in [24], at the interface $x = \xi$, we obtain E_z and its first derivative with respect to x is continuous:

$$E_z(\xi^-, t) = E_z(\xi^+, t),$$

$$\frac{\partial}{\partial x} E_z(\xi^-, t) = \frac{\partial}{\partial x} E_z(\xi^+, t).$$

These two conditions are sufficient to determine the values of magnitudes A_1 and A_2, if $\omega_{x,1}$ and $\omega_{x,2}$ are known.

It is of great interest to consider the 2nd-order jump condition, which originally involves the y derivative as in Eq. (16). In the present context, it can be verified from Eq. (21) that the second

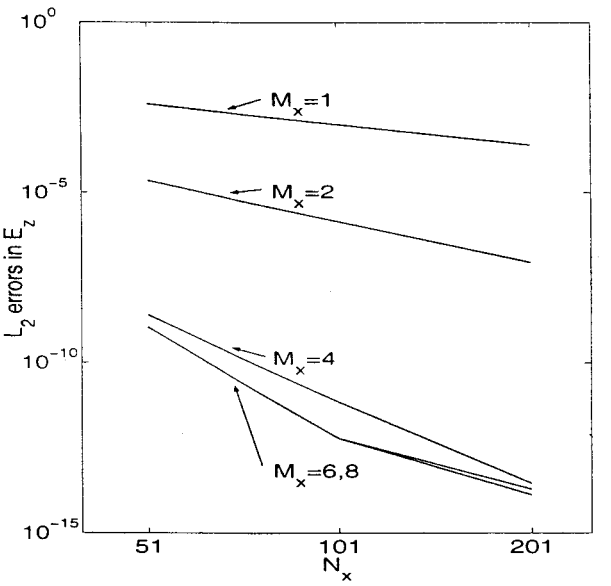

(a)

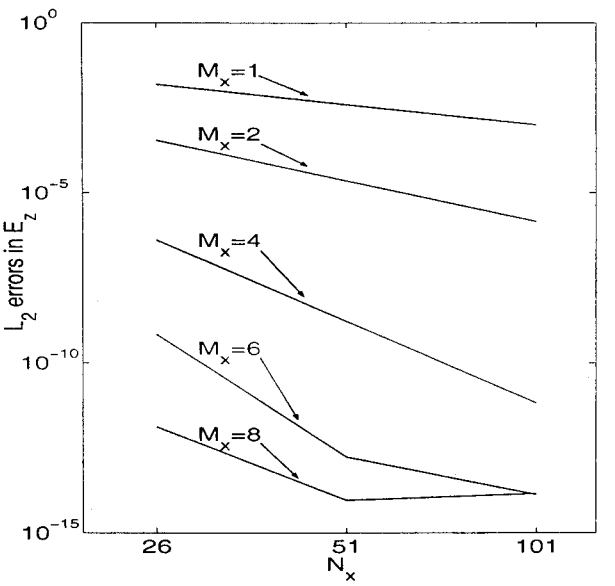

(b)

Figure 2 Log-log plots of the L_2 errors in E_z at time $t = 1$ by using the FDTD method for different M_x values ($\Delta t = 2.5 \times 10^{-4}$ and $M_y = 8$): (a) 2D HDM method with $l = 8$; (b) TPDM method

derivative of E_z with respect to x is discontinuous at the interface; furthermore, we obtain the relation

$$\frac{1}{\omega_{x,1}^2}\frac{\partial^2}{\partial x^2}E_z(\xi^-, t) = \frac{1}{\omega_{x,2}^2}\frac{\partial^2}{\partial x^2}E_z(\xi^+, t). \tag{22}$$

It is interesting to note that condition (22) is almost identical to the 2nd-order jump condition for E_z in the 1D case, that is, Eq. (7), except that ε_1 and ε_2 are replaced with $\omega_{x,1}^2$ and $\omega_{x,2}^2$, respectively. In fact, it can be derived that the field E_z given by Eq. (21) satisfies any-order jump condition for E_z, as in the 1D case after replacing ε_1 and ε_2 with $\omega_{x,1}^2$ and $\omega_{x,2}^2$, respectively. This set of jump conditions can then be used to determine as many FPs along the x direction as one wants, in principle. This suggests that it is possible to extend the 1D DM method directly to 2D tensor-product geometries by simply considering parameters $\omega_{x,1}^2$ and $\omega_{x,2}^2$, but not permittivities ε_1 and ε_2. For example, we can rewrite condition (22) as

$$\frac{\partial^2}{\partial x^2}E_z(\xi^-, t) = \frac{\omega_{x,1}^2}{\omega_{x,2}^2}\frac{\partial^2}{\partial x^2}E_z(\xi^+, t). \tag{23}$$

It is clear from Eq. (23) that the factor $R = \omega_{x,1}^2/\omega_{x,2}^2$ determines the relationship. In the 1D case, we have $\omega_y = 0$. Thus,

$$R = \frac{\omega_{x,1}^2}{\omega_{x,2}^2} = \frac{\varepsilon_1\omega^2 - \omega_y^2}{\varepsilon_2\omega^2 - \omega_y^2} = \frac{\varepsilon_1\omega^2}{\varepsilon_2\omega^2} = \frac{\varepsilon_1}{\varepsilon_2}. \tag{24}$$

In other words, the factor R solely depends on the material permittivities in the 1D cases. This actually justifies the soundness of the present 2D considerations. On the other hand, by itself, Eq. (24) also provides clear evidence about why the 1D DM method is difficult to be directly generalized to 2D studies, or why the 1D DM method is much easier than that of 2D. What simply relates x derivatives of E_z component is the factor in terms of wave numbers: $R = \omega_{x,1}^2/\omega_{x,2}^2$, which, however, is generally unknown. As a consequence, the jump conditions containing ε_1 and ε_2 inevitably involve y derivatives and cross derivatives, so that the 2D DM modeling is extremely complicated. In contrast, the factor R happens to be equal to the known factor of material property $\varepsilon_1/\varepsilon_2$ in 1D cases, so that 1D DM modeling can be easily carried out.

This investigation motivates us to design a new tensor-product derivative-matching (TPDM) method for simple 2D cases. The basic consideration is to numerically estimate the factor R for 2D problems. We denote such an estimate as $\bar{R}$. Whenever $\bar{R}$ is computed, the well-developed 1D IDM method [24] can be directly employed for 2D applications. Note that the stability constraint of the TPDM is thus the same as that of the 1D IDM method, which was carefully studied in [24]. In order to estimate R, we must assume that the initial solutions of the time-domain problem under consideration are analytically available. In each homogeneous region, we consider a highly accurate approximation of $\partial^2 E_z/\partial x^2$ at one grid node. By dividing such an approximation with the corresponding initial value of E_z at that node, we attain an estimate of $-\omega_{x,1}^2$ or $-\omega_{x,2}^2$. The estimate of R can thus be easily generated.

An advantage of the TPDM is that it is very efficient for the numerical simulation of long-time wave propagation, because of its preprocessing nature. It is noted that although the TPDM is formulated on a uniform grid, it actually works on more general grid settings, that is, either staggered or nonstaggered grid systems, as well as the domain-decomposition setting. In general, it can be employed together with any time-domain solver. Moreover, a nonuniform grid can be applied near the interface to enhance adaptivity with appropriate Lagrange coefficients of differentiation.

It is noted that because an accurate estimate of $\bar{R}$ is generally impossible for many CEM problems, such as time-domain wave-scattering problems [15, 16] and frequency-domain problems [17, 27], the proposed TPDM method cannot be applied to these situations. Moreover, the relation becomes more complicated in 3D. In other words, it is not a generally applicable approach for CEM. However, the TPDM method does provide accurate approximations for initial guided-wave problems. In practice, it is also found the accuracy of the TPDM method crucially depends on the accuracy in the estimation of $\bar{R}$. Even though the TPDM method can only be applied to a limited class of CEM applications, once it is applicable, it can be much more effective than our previous

TABLE 2 L_2 Errors of the FDTD Methods with the TPDM at Time $t = 0.5$ with $\Delta t = 1.0 \times 10^{-4}$ at High-Frequency Parameter Setting ($M_y = 8$)

		E_z		H_x		H_y	
M_x	(N_x, N_y)	Error	Rate	Error	Rate	Error	Rate
1	(26, 21)	3.69(−1)		4.26(−1)		7.33(−1)	
	(51, 41)	1.90(−1)	0.953	1.30(−1)	1.709	2.81(−1)	1.379
	(101, 81)	6.42(−2)	1.569	2.54(−2)	2.355	5.57(−2)	2.339
2	(26, 21)	1.98(−1)		2.53(−1)		5.35(−1)	
	(51, 41)	3.46(−2)	2.517	1.34(−2)	4.234	2.94(−2)	4.181
	(101, 81)	2.38(−3)	3.861	8.36(−4)	4.006	1.82(−3)	4.014
4	(26, 21)	1.34(−1)		8.21(−2)		1.80(−1)	
	(51, 41)	1.40(−3)	6.583	5.15(−4)	7.317	1.11(−3)	7.340
	(101, 81)	6.68(−6)	7.710	2.43(−6)	7.728	5.25(−6)	7.723
6	(26, 21)	7.41(−2)		3.62(−2)		7.83(−2)	
	(51, 41)	7.75(−5)	9.900	2.85(−5)	10.307	6.14(−5)	10.315
	(101, 81)	2.70(−8)	11.482	9.88(−9)	11.497	2.13(−8)	11.492
8	(26, 21)	4.19(−2)		1.87(−2)		4.01(−2)	
	(51, 41)	4.95(−6)	13.047	1.81(−6)	13.333	3.92(−6)	13.318
	(101, 81)	1.36(−10)	15.147	4.87(−11)	15.185	1.05(−10)	15.176

TABLE 3 L_2 Errors of the FDTD Method with the TPDM at Time $t = 1$ with $\Delta t = 2.5 \times 10^{-4}$ ($M_x = M_y = 8$, $N_x = 51$, and $N_y = 41$)

$\lvert R - \bar{R}\rvert$	E_z	H_x	H_y
1.00(−14)	8.80(−15)	4.01(−15)	8.92(−15)
1.00(−10)	1.11(−12)	4.66(−13)	1.02(−12)
1.00(−6)	1.11(−8)	4.63(−9)	1.01(−8)
1.00(−2)	1.10(−4)	4.62(−5)	1.01(−4)

Q4DM and HDM methods, in terms of accuracy, simplicity, and efficiency.

3. NUMERICAL STUDIES

We numerically investigate the performance and analyze the limitation of the proposed FDTD TPDM scheme for 2D electromagnetic applications in this section. The two previous high-order schemes, the Q4DM and 2D HDM methods, are also employed for a comparison. We use the 4th-order Runge–Kutta scheme for time integration. Standard staggered grids are used in this work. Boundary extension techniques [15–17, 27] are used to impose the PEC conditions.

The first problem being considered has a PEC-bounded domain $\Omega = \{(x, y) | 0 \le x \le 5/4,\ 0 \le y \le 1\}$. The permittivity is defined by

$$\varepsilon = \begin{cases} \varepsilon_2, & \text{if } 0 \le x \le \dfrac{1}{2}, \quad 0 \le y \le 1, \\ \varepsilon_1, & \text{if } \dfrac{1}{2} \le x \le \dfrac{5}{4}, \quad 0 \le y \le 1. \end{cases}$$

The exact solution for time-varying electromagnetic fields is given by [21]:

$$E_z = \begin{cases} \sin(a_1 x)\sin(by)\sin(\omega t), & 0 \le x \le \dfrac{1}{2} \quad 0 \le y \le 1, \\ \cos(a_2 x)\sin(by)\sin(\omega t), & \dfrac{1}{2} \le x \le \dfrac{5}{4} \quad 0 \le y \le 1. \end{cases}$$

$$H_y = \begin{cases} -\dfrac{a_1}{\omega}\cos(a_1 x)\sin(by)\cos(\omega t), & 0 \le x \le \dfrac{1}{2} \quad 0 \le y \le 1, \\ \dfrac{a_2}{\omega}\sin(a_2 x)\sin(by)\cos(\omega t), & \dfrac{1}{2} \le x \le \dfrac{5}{4} \quad 0 \le y \le 1. \end{cases}$$

$$H_x = \begin{cases} \dfrac{b}{\omega}\sin(a_1 x)\cos(by)\cos(\omega t), & 0 \le x \le \dfrac{1}{2} \quad 0 \le y \le 1, \\ \dfrac{b}{\omega}\cos(a_2 x)\cos(by)\cos(\omega t), & \dfrac{1}{2} \le x \le \dfrac{5}{4} \quad 0 \le y \le 1, \end{cases}$$

where $a_1^2 + b^2 = \varepsilon_2\omega^2$, $a_2^2 + b^2 = \varepsilon_1\omega^2$, $\sin(a_1/2) = \cos(a_2/2)$, and $\cos(5a_2/4) = 0$. As in [21], the set of parameters to be tested is chosen as $\varepsilon_1 = 1$, $\varepsilon_2 = 2$, $a_1 = 3\pi$, $a_2 = 2\pi$, $b = \pi$, and $\omega = \sqrt{5}\,\pi$.

We evaluate the performance of the TPDM method. For the chosen set of problem parameters, we have $R = \omega_{x,1}^2/\omega_{x,2}^2 = a_1^2/a_2^2 = 9/4$. By using the standard FD approximations to the 2nd-order derivative with $M_x = 16$ in each homogeneous region, a highly accurate estimate of R can be made. The numerical error in the estimation is found to be as small as $\lvert R - \bar{R}\rvert = 2.22 \times 10^{-14}$ by using a coarse grid with $\Delta x = 0.025$. With such an accurate estimation, satisfactory results are obtained by using the TPDM method (see Table 1 and Fig. 2). It is clear from Table 1 that theoretical order of accuracy is numerically confirmed for $M_x = 1$, 2, 4, and 6, until the machine limit is reached. For $M_x = 8$, its convergence rate is obviously restricted by the double precision. Therefore, when it is applicable, the TPDM method can achieve higher order of accuracy than our previous 2D HDM method, as shown in Figure 2. Furthermore, it is noted that the TPDM method also performs very well if one's computational nodes are not on the interface $x = \xi$. Results of equal quality are obtained, although they are not reported.

As the convergence in Table 1 is limited by the machine precision, we next consider a set of parameters which are more difficult to compute due to the presence of high-frequency waves. We choose $\varepsilon_1 = 1$, $\varepsilon_2 = 261/136$, $a_1 = 15\pi$, $a_2 = 10\pi$, $b = 6\pi$, and $\omega = 2\sqrt{34}\ \pi$. The numerical results for this set of parameters are listed in Table 2. Note that in this case we also have $R = a_1^2/a_2^2 = 9/4$. As expected, our numerical rate of convergence is close to the designed one, namely, 16.

Next, we explore the limitation of the TPDM method. To this end, the influence of the accuracy in estimating $\bar{R}$ for the final numerical results of the TPDM method is examined. To demonstrate this influence, we artificially enlarge the estimation error $\lvert R - \bar{R}\rvert$ for the first set of problem parameters. Four different $\bar{R}$ values with different errors are tested (see Table 3). It is found from Table 3 that the accuracy of the entire scheme proportionately deteriorates as the estimation error increases. In other words, if an accurate estimate $\bar{R}$ is unavailable, the performance of the TPDM method is quite poor. Therefore, we point out that the TPDM method has a limitation for general electromagnetic applications.

It is important to verify that the proposed method works for different test problems. For this purpose, we further examine the numerical performance of the TPDM scheme by considering another 2D CEM problem. In this problem, a lossless dielectric region with a relative permittivity of ε_2 is enclosed by air in the x direction, and the media are nonmagnetic and homogeneous along the y direction. The computational domain $\Omega = \{(x, y) | \lvert x\rvert \le 1, \lvert y\rvert \le 1\}$ is enveloped by PEC walls. The permittivity is given as

$$\varepsilon = \begin{cases} \varepsilon_2, & \text{if } \dfrac{1}{2} \le |x| \le 1, \quad |y| \le 1, \\ \varepsilon_1, & \text{if } |x| \le \dfrac{1}{2}, \quad |y| \le 1, \end{cases}$$

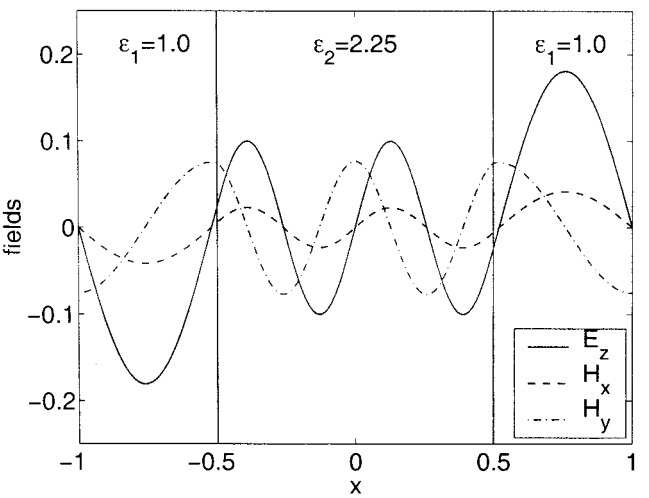

Figure 3 Plots of electromagnetic fields along the line $y = 1/3$ at time $t = 0.75$

where $\varepsilon_1 = 1$ and $\varepsilon_1 = 2.25$. This problem admits an exact solution for the following time-varying electromagnetic fields:

$$E_z = \begin{cases} \sin\left(\frac{\omega_2}{2}\right)\sin(\omega_1(x+1))\sin(\omega_y y)\cos(\omega t), & -1 \le x < -\frac{1}{2} \quad |y| \le 1 \\ -\sin\left(\frac{\omega_1}{2}\right)\sin(\omega_2 x)\sin(\omega_y y)\cos(\omega t), & -\frac{1}{2} \le x \le \frac{1}{2} \quad |y| \le 1 \\ \sin\left(\frac{\omega_2}{2}\right)\sin(\omega_1(x-1))\sin(\omega_y y)\cos(\omega t), & \frac{1}{2} < x \le 1 \quad |y| \le 1 \end{cases},$$

$$H_x = \begin{cases} -\frac{\omega_y}{\omega}\sin\left(\frac{\omega_2}{2}\right)\sin(\omega_1(x+1))\cos(\omega_y y)\sin(\omega t), & -1 \le x < -\frac{1}{2} \quad |y| \le 1 \\ \frac{\omega_y}{\omega}\sin\left(\frac{\omega_1}{2}\right)\sin(\omega_2 x)\cos(\omega_y y)\sin(\omega t), & -\frac{1}{2} \le x \le \frac{1}{2} \quad |y| \le 1 \\ -\frac{\omega_y}{\omega}\sin\left(\frac{\omega_2}{2}\right)\sin(\omega_1(x-1))\cos(\omega_y y)\sin(\omega t), & \frac{1}{2} < x \le 1 \quad |y| \le 1 \end{cases},$$

$$H_y = \begin{cases} \frac{\omega_1}{\omega}\sin\left(\frac{\omega_2}{2}\right)\cos(\omega_1(x+1))\sin(\omega_y y)\sin(\omega t), & -1 \le x < -\frac{1}{2} \quad |y| \le 1 \\ -\frac{\omega_2}{\omega}\sin\left(\frac{\omega_1}{2}\right)\cos(\omega_2 x)\sin(\omega_y y)\sin(\omega t), & -\frac{1}{2} \le x \le \frac{1}{2} \quad |y| \le 1 \\ \frac{\omega_1}{\omega}\sin\left(\frac{\omega_2}{2}\right)\cos(\omega_1(x-1))\sin(\omega_y y)\sin(\omega t), & \frac{1}{2} < x \le 1 \quad |y| \le 1 \end{cases},$$

where $\omega_1^2 + \omega_y^2 = \varepsilon_1\omega^2$ and $\omega_2^2 + \omega_y^2 = \varepsilon_2\omega^2$. Here, the value of ω can be determined according to the relation

$$\sqrt{\varepsilon_2\omega^2 - \omega_y^2}\tan\left(\frac{\sqrt{\varepsilon_1\omega^2 - \omega_y^2}}{2}\right) = \sqrt{\varepsilon_1\omega^2 - \omega_y^2}\tan\left(-\frac{\sqrt{\varepsilon_2\omega^2 - \omega_y^2}}{2}\right).$$

We choose $\omega_y = 2\pi$ to satisfy the PEC conditions on $y = \pm 1$. Correspondingly, $\omega \approx 9.07716175885174$. The analytical solution is depicted in Figure 3.

We are particularly interested in a comparison with our previous two high-order schemes, the Q4DM and HDM. Numerical results of the three schemes for this test case are listed in Table 4. The Q4DM scheme produces essentially the designed 4th order of accuracy. The HDM scheme with both $M_x = 6$ and $M_x = 8$ yields almost the same accuracy and convergence rate, showing the limitation of its iterative procedure. The highest order of accuracy of the HDM method is about 12th order, as shown in Table 4. For the TPDM method, the designed convergence order is reached numerically for $M_x = 6$, while the numerical rate of $M_x = 8$ is affected by the limit of double precision. As can be seen from Table 4, the TPDM method is clearly the most accurate scheme among the three tested methods.

The CPU time of three methods is also given in Table 4. The CPU time of the Q4DM method is the smallest among three methods. However, if the same accuracy level is required to be achieved for three methods, the TPDM is the most cost-efficient

TABLE 4 L_2 Errors of the FDTD Method at Time $t = 1$ with $\Delta t = 2.0 \times 10^{-4}$ for All Three DM Schemes ($M_y = 8$ and $M_x = m$)

				E_z		H_x		H_y		
Scheme	M_x	l	(N_x, N_y)	Error	Rate	Error	Rate	Error	Rate	CPU
Q4DM	2	—	(21,21)	1.15(−4)		1.12(−4)		1.86(−4)		6.86
			(41,41)	7.53(−6)	3.932	7.34(−6)	3.937	1.18(−5)	3.973	23.16
HDM	6	8	(21,21)	1.83(−6)		9.92(−7)		1.50(−6)		11.28
			(41,41)	5.50(−10)	11.697	2.48(−10)	11.967	4.00(−10)	11.868	34.73
	8	8	(21,21)	1.84(−6)		9.98(−7)		1.51(−6)		15.05
			(41,41)	5.50(−10)	11.706	2.48(−10)	11.976	4.00(−10)	11.880	41.56
TPDM	6	6	(21,21)	1.70(−9)		1.47(−9)		2.49(−9)		9.90
			(41,41)	4.73(−13)	11.812	4.15(−13)	11.794	6.99(−13)	11.798	30.77
	8	8	(21,21)	1.43(−11)		2.36(−11)		3.41(−11)		14.32
			(41,41)	6.90(−15)	11.013	6.99(−15)	11.719	9.67(−15)	11.784	39.84

CPU time is reported in seconds. Note that the definition of l in the TPDM method follows from the 1D HDM method, thus it differs from that of the 2D HDM method.

method, as it can be about 2000 times more efficient than the Q4DM scheme.

4. CONCLUSION

This paper has proposed a tensor-product derivative matching (TPDM) scheme to extend the 2D finite-difference time-domain (FDTD) method to a high order of accuracy with the presence of material interface. The proposed method makes use of a systematic procedure, that is, implicit derivative matching [24] to construct numerical schemes that greatly exceed the convergence rate of the previous 4^{th}-order methods [4, 20–23]. The proposed scheme is designed to overcome certain drawback of our previous two high-order methods, quasi-4^{th}-order derivative matching (Q4DM) and 2D hierarchical derivative matching (HDM) [24], whose order of accuracy is limited by its iterative nature. Moreover, the 2D HDM scheme requires the interface to be on the grid points, which limits its application to grid systems more complex than the body-fitted ones. Similar to our previous high-order schemes, the proposed TPDM approach utilizes fictitious points, a technique used by Driscoll and Fornberg in their block pseudospectral methods [25, 26] to locally modify the differential stencils near the material interfaces based on a structured grid. Moreover, we locally modify the differential stencils at the beginning, the so-called preprocessing stage, which is attractive for long time integration. Two numerical examples are chosen to test the performance of the proposed TPDM scheme and to compare it with our previous Q4DM and 2D HDM methods. The numerical results indicate that the new method could reach a nearly 16^{th} order of accuracy for wave propagation with material interfaces. When applicable, the proposed TPDM can be about 2000 times more efficient than our previous Q4DM approach.

REFERENCES

1. K.S. Yee, Numerical solution of initial boundary value problems involving Maxwell's equations in isotropic media, IEEE Trans Antennas Propagat 14 (1966), 302–306.
2. A. Taflove and S.C. Hagness, Computational electrodynamics: The finite-difference time-domain method, 2nd ed., Artech House, Boston–London, 2000.
3. Q.H. Liu, The PSTD algorithm: A time-domain method requiring only two cells per wavelength, Microwave Opt Technol Lett 15 (1997), 158–165.
4. J.S. Hesthaven, High-order accurate methods in time-domain computational electromagnetics: A review, Adv Imaging Electron Phys 127 (2003), 59–123.
5. R. Holland, Finite difference solutions of Maxwell's equations in generalized nonorthogonal coordinates, IEEE Trans Nuclear Sci 30 (1983), 4589–4591.
6. K.S. Yee, J.S. Chen, and A.H. Chang, Conformal finite difference time-domain (FDTD) with overlapping grids, IEEE Trans Antennas Propagat 40 (1992), 1068–1075.
7. T.G. Jurgens, A. Taflove, K. Umashaankar, and T.G. Moore, Finite difference time-domain modeling of curved surfaces, IEEE Trans Antennas Propagat 40 (1992), 357–366.
8. P.G. Petropoulos, Phase error control for FD-TD methods of second and fourth order accuracy, IEEE Trans Antennas Propagat 24 (1994), 859–862.
9. D.W. Zingg, H. Lomax, and H. Jurgens, High-accuracy finite-difference schemes for linear wave propagation, SIAM J Sci Comput 17 (1996), 328–346.
10. J.L. Young, D. Gaitonde, and J.S. Shang, Towards the construction of a fourth order difference scheme for transient EM wave simulation: Staggered grid approach, IEEE Trans Antennas Propagat 45 (1997), 1573–1580.
11. E. Turkel, High-order methods, Advances in computational electrodynamics: The finite-difference time-domain method, A. Taflove (Editor), Artech House, Boston, 1998, ch. 2.
12. E. Turkel and A. Yefet, On the construction of a high order difference scheme for complex domains in a Cartesian grid, Appl Numer Math 33 (2000), 113–124.
13. Q. Li, Y. Chen, and D. Ge, Comparison study of the PSTD and FDTD methods for scattering analysis, Microwave Opt Technol Lett 25 (2000), 220–226.
14. Z.H. Shao, Z. Shen, Q. He, and G.W. Wei, A generalized higher-order finite-difference time-domain method and its application in guided-wave problems, IEEE Trans Microwave Theory Tech 51 (2003), 856–861.
15. G. Bao, G.W. Wei, and S. Zhao, Local spectral time-domain method for electromagnetic wave propagation, Optics Lett 28 (2003), 513–515.
16. Z.H. Shao, G.W. Wei, and S. Zhao, DSC time-domain solution of Maxwell's equations, J Comput Phys 189 (2003), 427–453.
17. G. Bao, G.W. Wei, and S. Zhao, A new approach for computational electromagnetics, IEEE Trans Antennas Propagat (to appear).
18. A. Ditkowski, K. Dridi, and J.S. Hesthaven, Convergent Cartesian grid methods for Maxwell's equations in complex geometries, J Comput Phys 170 (2001), 39–80.
19. W. Cai and S.Z. Deng, An upwinding embedded boundary method for Maxwell's equations in media with material interfaces: 2D case, J Comput Phys 190 (2003), 159–183.
20. A. Yefet and E. Turkel, Fourth order compact implicit method for the Maxwell equations with discontinuous coefficients, Appl Numer Math 3 (2000), 125–134.
21. A. Yefet and P.G. Petropoulos, A non-dissipative staggered fourth order accurate explicit finite difference scheme for the time-domain Maxwell's equations, J Comput Phys 168 (2001), 286–315.
22. Z.Q. Xie, C.-H. Chan, and B. Zhang, An explicit fourth order staggered finite-difference time-domain method for Maxwell's equations, J Comput Appl Math 147 (2002), 75–98.
23. Z.Q. Xie, C.-H. Chan, and B. Zhang, An explicit fourth order orthogonal curvilinear staggered-grid FDTD method for Maxwell's equations, J Comput Phys 175 (2002), 739–763.
24. S. Zhao and G.W. Wei, High-order FDTD methods via derivative matching for Maxwell's equations with material interfaces, preprint available at http://www.math.ntnu.no/conservation/2003/064.html.
25. T.A. Driscoll and B. Fornberg, A block pseudospectral method for Maxwell's equations, Pt. I: One-dimensional case, J Comput Phys 140 (1998), 47–65.
26. T.A. Driscoll and B. Fornberg, Block pseudospectral methods for Maxwell's equations, Pt. II: Two-dimensional, discontinuous-coefficient case, SIAM J Sci Comput 21 (1999), 1146–1167.
27. G. Bao, G.W. Wei, and S. Zhao, Numerical solution of the Helmholtz equation with high wavenumbers, Int J Numer Meth Eng 59 (2004), 389–408.

WIDEBAND HEXAGONAL-SHAPE STACKED-PATCH ANTENNA ARRAY WITH L-PROBE FEED

Steven S. L. Yang and K. M. Luk
Department of Electronic Engineering
City University of Hong Kong
83 Tat Chee Avenue
Kowloon, Hong Kong SAR

Received 9 March 2004

ABSTRACT: *A two-element hexagonal-shape stacked-patch antenna array fed by an L-shaped probe is designed and measured. Experimental results show that the array achieves an impedance bandwidth of 34%*